



Status of the MINOS Experiment

M.A. Thomson^a

^aCavendish Laboratory, University of Cambridge, Cambridge CB3 0HE, England

MINOS is a long baseline neutrino oscillation experiment utilising the NuMI beam at Fermilab. The main goal of the experiment is to probe the region of parameter space responsible for atmospheric neutrino oscillations. This paper gives an overview of the beam, the MINOS detectors and the main physics goals of the experiment. The NuMI beam is currently being installed at Fermilab and is due to be commissioned at the end of 2004. However, the MINOS far detector has been recording data since the beginning of August 2003 and as an illustration of the physics capabilities of the MINOS detector, this paper presents the first observations of ν_μ and $\bar{\nu}_\mu$ charged current atmospheric neutrino interactions.

1. Introduction

During the past ten years the phenomenon of atmospheric neutrino oscillation has been firmly established by the Super-Kamiokande experiment [1] and confirmed by MACRO [2] and Soudan 2 [3]. The favoured interpretation of the data is $\nu_\mu \leftrightarrow \nu_\tau$ neutrino oscillations. Recent results from Super-Kamiokande [4, 5] provide 90% confidence level constraints on $(\Delta m_{23}^2, \sin^2 2\theta_{23})$ of $1.9 \times 10^{-3} \text{eV}^2 < \Delta m_{23}^2 < 3.0 \times 10^{-3} \text{eV}^2$, and $\sin^2 2\theta_{23} > 0.90$. The main aim of the MINOS experiment is to probe this region of parameter space and to make a precise measurement of Δm_{23}^2 in a high statistics beam experiment.

The MINOS (Main Injector Neutrino Oscillation Search) experiment [6] will utilise the intense ν_μ NuMI (Neutrinos at the Main Injector) beam which is currently being constructed at Fermilab. The neutrinos pass through the Earth and are detected at a distance of 735 km in the 5.4 kton MINOS Far Detector which is located at a depth of 714 m in the Soudan mine, Northern Minnesota. A 1 kton near detector is located at a distance of 1 km. The near detector is similar in design to the far detector, and due to space constraints is not discussed in this paper. By comparing the observed neutrino energy spectrum in the far detector (which includes the effects of neutrino oscillations) to the unoscillated spectrum in the near detector the oscillation minimum can be resolved

yielding a 10% measurement of Δm_{23}^2 .

Construction of the NuMI beam is in an advanced state, with first beam expected late 2004/early 2005. The MINOS near detector was completed during summer 2004 and is currently being commissioned. The completed MINOS far detector has been recording high quality data since the beginning of August 2003. These data are used to perform a preliminary study of atmospheric neutrinos interactions. Given the limited exposure, no attempt to extract oscillation parameters is made at this stage.

2. The NuMI Beam

The NuMI neutrino beam is produced using 120 GeV protons from the Fermilab Main Injector (MI). Every 1.9 s protons are extracted from the MI in a single turn (8.7 μs). In order for the neutrino beam to be directed towards the Soudan mine its trajectory is required to point 58 mrad downward. However, for civil construction reasons, the MINOS target hall and meson decay tunnel is located in the dolomite rock formation approximately 50 m below the surface. For this reason the extracted protons are first bent steeply downward into the dolomite rock before being steered to the correct pitch. The proton beam then impinges on a slim segmented graphite target. The charged mesons (predominantly π^\pm, K^\pm) produced in the target are fo-

cused by two neutrino horns with parabolic inner conductors. The horns are pulsed with a current of 200 kA which produces a toroidal magnetic field, $B \sim I/r$, between the inner and outer conductors. The direction of the current is such that positive particles are focused and negative particles defocused. The pions and kaons then decay in a 675 m long decay pipe of radius 1 m which is evacuated to 1.5 Torr.

One important feature of the NuMI beam is its flexibility. The two horns behave as a pair of highly achromatic lenses; the separation of the two horns and the location of the target, all of which can be adjusted, determines the energy spectrum of the focused mesons. The resulting neutrino spectra for three different horn configurations are shown in Figure 1. For the NuMI/MINOS baseline of 735 km, the Super-Kamiokande results suggest that the first oscillation minimum will occur for neutrino energies in the range 1.0–2.5 GeV. Consequently, the low energy horn configuration will be used for the initial physics running.

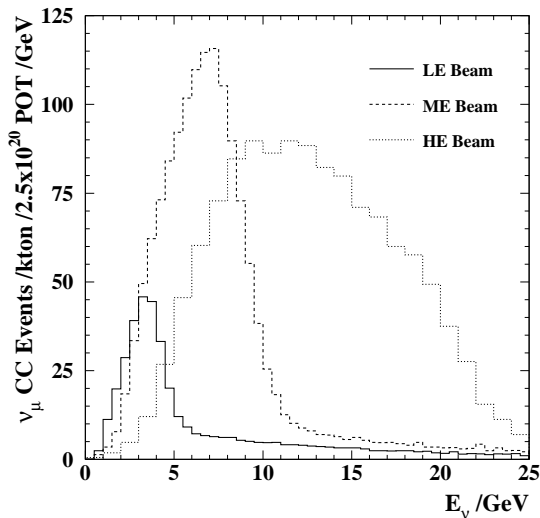


Figure 1. Expected number of ν_μ CC interactions /kton / 2.5×10^{20} protons on target /GeV for three different horn configurations: low Energy (LE), medium energy (ME) and high energy (HE).

The majority of the beam components are installed and the beam will be commissioned at the end of 2004. It is anticipated that the machine will operate with a beam intensity of 2.5×10^{13} protons per pulse corresponding to 2.5×10^{20} protons per year; a beam power of 0.3 MW. It is important to note that the MINOS physics sensitivity depends on the total number of protons on target and a number of schemes to increase the proton intensity are being considered.

3. The MINOS Far Detector

The MINOS far detector is a 5.4 kton steel-scintillator sampling calorimeter consisting of two super-modules (SM) separated by a gap of 1.1 m. The basic detector structure consists of octagonal planes of 2.54 cm thick steel followed by planes of 1 cm thick scintillator and a 2 cm wide air gap. The first and second SMs are comprised of 248 and 236 scintillator planes respectively. Each SM is magnetised to an average value of 1.5 T by a 15 kA current loop which runs along the coil hole along the detector central axis and returns below the detector. Each scintillator plane is made up of 192 optically isolated 4 cm wide strips of length up to 8 m depending on the position in the plane. The strips in alternating planes are oriented at $\pm 45^\circ$ to the vertical thereby providing two orthogonal coordinates, $U = \frac{1}{\sqrt{2}}(x + y)$ and $V = \frac{1}{\sqrt{2}}(x - y)$. The scintillation light is collected using wavelength shifting (WLS) fibres embedded within the scintillator strips. The WLS fibres are coupled to clear optical fibres at both ends of a strip and are read out using 16-pixel multi-anode photomultiplier tubes (PMTs). Each PMT pixel reads out eight strips separated by approximately 1 m within the same plane. The resulting eight-fold ambiguity is resolved in software.

The detector is optimised for beam neutrinos coming from the direction of Fermilab. For the study of atmospheric neutrinos (see below) the planar structure presents a particular problem; cosmic-ray muon events travelling almost parallel to the planes can penetrate deep into the detector by travelling in the steel or air between the planes. To reject this source of background, a scintillator veto shield surrounds the upper part

of the detector. The veto shield consists of one or two scintillator planes constructed out of the same modules as used in the main detector. The veto shield is constructed in 4 sections (two above SM1 and two above SM 2) which overlap in the z -direction.

3.1. Data Acquisition and Trigger

The output signals from each pixel are digitised and time-stamped (with a 1.5 ns precision) in the VME-based front-end electronics. The signals from the PMTs are digitised by 14-bit analogue-to-digital converters when the dynode signal from the PMT exceeds a programmable threshold. To reduce the data flow, the pedestal corrected signals are only written to the DAQ output buffers if they exceed a programmable threshold. The raw data rate is approximately 8 MB s^{-1} . The raw data are transferred to a PC based trigger farm. The data are divided into blocks which are bounded by regions of 100 clock ticks (156 ns) where there is no read out detector activity. The primary MINOS trigger algorithm is to require activity in at least 4 planes out of any contiguous group of 5 planes within a window of 200 ns. The veto shield is read out in the same way as the far detector.

3.2. Detector Calibration

A minimum ionising particle crossing at normal incidence to a plane gives a combined signal of approximately 10 photo-electrons (PEs) registered by the PMTs at the two ends of the strip. The detector is calibrated using both a dedicated LED system and cosmic ray muons. In this way the ADC values recorded by the PMTs are converted into an equivalent number of PEs. Cosmic ray muons are also used to calibrate the recorded times. After calibration, a single hit timing resolution of approximately 2.5 ns is achieved.

4. MINOS Physics goals

The main goals of the MINOS experiment are summarised below:

i) Although neutrino flavour oscillations provide a good description of the atmospheric neutrino data no experiment has yet to demonstrate con-

clusively the oscillatory nature of the expected signal (although evidence for an oscillation dip has been observed in the Super-Kamiokande [4] and K2K [7] data). The MINOS experiment will be able to observe the oscillation dip, as can be seen in Figure 2 and provide high statistics discrimination against possible alternative models *e.g.* decoherence and ν decay.

ii) The MINOS experiment will be able to provide a precise measurement of Δm_{23}^2 . Figure 2 shows the expected sensitivity for three different numbers of protons on target. A precision of order 10% is achievable.

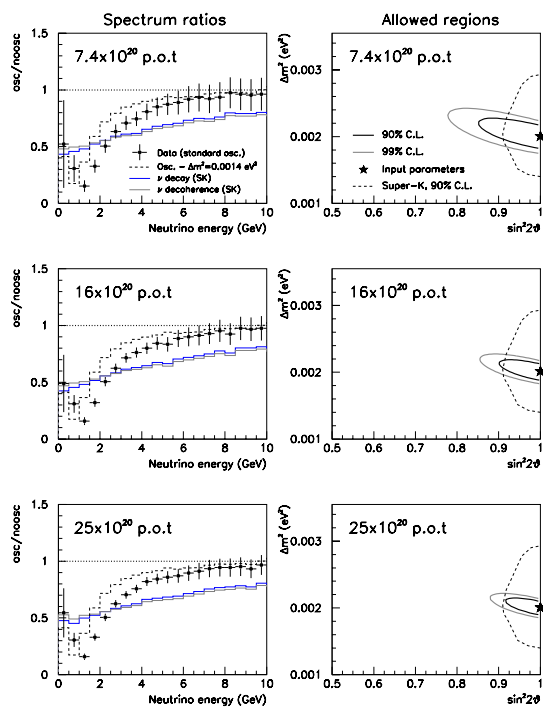


Figure 2. The left-hand plots show, for three different numbers of protons on target, the expected ratio of the reconstructed ν_μ energy spectrum in the far detector to that observed in the near detector assuming ($\Delta m_{23}^2 = 2.0 \times 10^{-3} \text{ eV}^2$, $\sin^2 2\theta_{23} = 1.0$). The right-hand plots show the corresponding expected 90% and 99% C.L. which include the expected systematic uncertainties.

iii) The MINOS experiment will search for subdominant $\nu_\mu \rightarrow \nu_e$ oscillations. The 3σ discovery extends beyond the CHOOZ limits [8] allowing possibility of the first measurement of θ_{13} . As an example of the potential experimental sensitivity of MINOS to θ_{13} , Figure 3 shows the three standard deviation discovery regions for three different integrated proton intensities. The ultimate experimental reach depends on the number of protons delivered to the target.

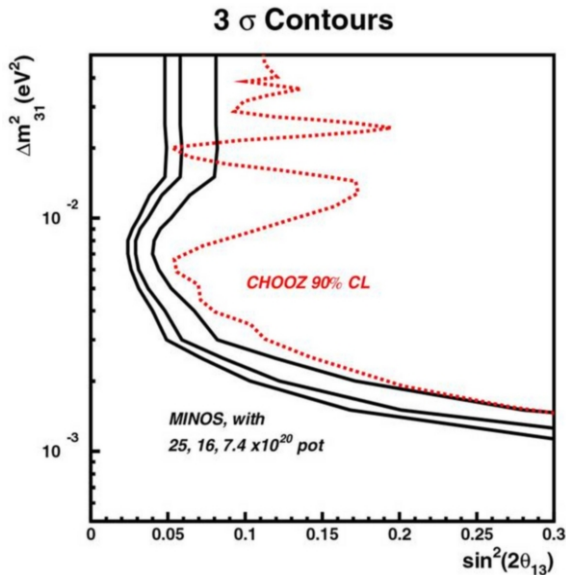


Figure 3. The MINOS three standard deviation discovery potential for a non-zero value of θ_{13} for three different total numbers of protons on target.

iv) The main goals of the MINOS experiment naturally involve the analysis of beam data. However, MINOS is the first large deep underground detector with a magnetic field. This allows charge current atmospheric neutrino interactions to be classified as either ν_μ or $\bar{\nu}_\mu$ from the curvature of the produced μ^\pm which tags the muon charge. This allows the possibility of studying neutrino flavour oscillations for neutrinos and anti-neutrinos separately. A separate measurement of ν_μ and $\bar{\nu}_\mu$ oscillations could provide constraints on CPT violating models [9, 10] which have been invoked to accommodate simultaneously the solar, atmospheric and LSND [11] neu-

trino oscillation data. It should be noted that a number of recent studies have indicated difficulties with the CPT violating models (see for example [12]). Nevertheless, a direct measurement of ν_μ and $\bar{\nu}_\mu$ oscillations is of experimental interest.

5. Far Detector Data Analysis

The MINOS far detector has been operational for more than a year and a significant sample of cosmic ray data has been accumulated. In addition, analyses for the atmospheric neutrinos have been developed. The data analysis chain is described below and the performance of the detector is highlighted.

5.1. Event Reconstruction

The first stage of the event reconstruction removes the eightfold ambiguity in the association of raw hits to strips. This is performed utilising information from both strip ends with timing used to resolve remaining ambiguities. For cosmic ray muons, on average 99% of the recorded charge is associated with the correct strip. At this stage the data are in the form of two 2D event views $U-z$ and $V-z$. Firstly, tracks and showers are reconstructed independently in each view; the two views are then matched to obtain a three-dimensional event. Figure 4 shows an example of a cosmic-ray muon in the MINOS far detector. The upper two plots show the strip versus plane information for the two event views, $U-z$ and $V-z$. The lower plot shows the $x-y$ projection after matching hits in the two views.

For cosmic-ray events which leave hits in both the veto shield and MINOS far detector, the root-mean-square difference in times recorded in veto shield and the detector is 15 ns, allowing association of veto shield hits to activity in the far detector. The event of Figure 4 has two veto shield hits which are associated both spatially and temporally with the event in the far detector.

5.2. Neutrino Reconstruction

Charged current muon neutrino events are reconstructed as muon tracks and hadronic showers. A typical 1 GeV muon will traverse approximately 25 planes at normal incidence. Typically, reconstructed tracks are required to con-

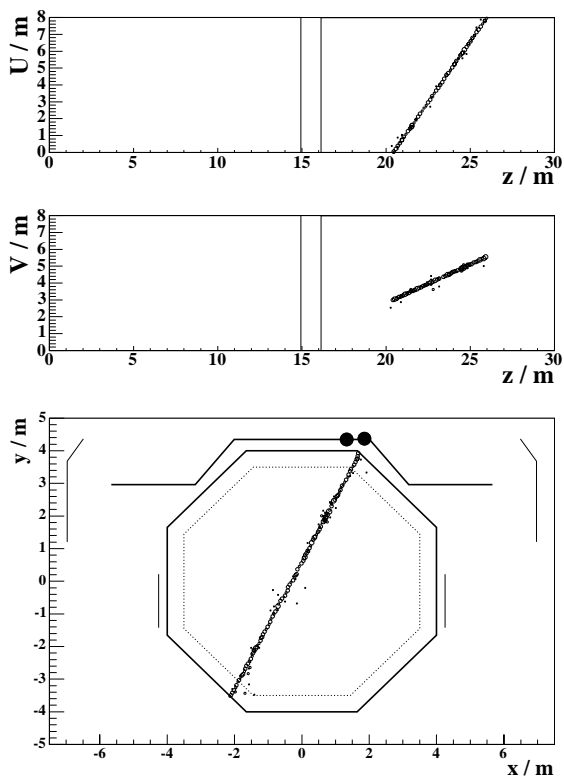


Figure 4. A through-going cosmic ray muon in the MINOS far detector. The size of the points gives an indication of the recorded hit charge. The lower plot shows both hits in the far detector and in-time hits in the veto shield.

sist of at least 8 planes (corresponding to a minimum energy of 0.4 GeV). For the contained event sample considered here the muon momentum is determined from range. The muon momentum resolution is approximately $(\sigma_p/p)^2 = 0.06^2 + (0.045/p(\text{GeV}))^2$ for muons travelling at normal incidence to the detector planes. The first term is dominated by fluctuations from energy loss and the second is dominated by sampling. The hadronic energy is obtained by summing the charge in a shower which is spatially associated with the start of the track. The energy scale is obtained from Monte Carlo using the GCALOR [13] model of hadronic showers. The hadronic response of the MINOS detector has been studied in a test beam experiment at CERN and GCALOR is found to provide a good

description of the detector response to single π^\pm and protons. The hadronic energy resolution is approximately $\sigma_E/E \sim 0.55/\sqrt{E/\text{GeV}}$.

For the study of atmospheric neutrinos it is necessary to determine whether the reconstructed track is upward or downward going. This is achieved by comparing the hit times along the reconstructed track with the hypotheses that it is either upward or downward going (assuming that the particle is travelling at almost the speed of light). The hypothesis with the smallest χ^2 is chosen. In addition, the difference in the χ^2 values obtained for the two different hypothesis is a measure of the quality of the direction determination. A relativistic normal incidence particle traverses ten planes in approximately 2 ns which should be compared to the single hit resolution of 2.5 ns. The curvature of μ^+/μ^- tracks in the magnetic field allows the charge sign to be determined for muon momenta in the approximate range 1–100 GeV (depending on orientation with respect to the magnetic field).

6. Atmospheric Neutrino Data

This paper presents preliminary observations of atmospheric neutrino interactions in the MINOS far detector. Two event categories are considered: neutrino induced upward-going muons from neutrino interactions in the surrounding rock; and events where the neutrino interaction occurs within the detector volume. The analyses that have been developed for both categories of events are described briefly below. In both cases the dominant background is from cosmic-ray muons which enter the MINOS detector.

The upward going muon analysis uses data collected from September 2002 to May 2003 (only one detector super-module) and from July 2003 to April 2004 (both super-modules). The contained event analysis uses data recorded between August 2003 and April 2004 and corresponds a fiducial exposure of 1.85 kt years. The different data sets are due to the contained event analysis requiring that the veto shield is fully operational. The exposure for the upward-going analysis is approximately 1.75 times greater than for the contained event analysis.

6.1. Neutrino induced upward muons

Upward-going muons from neutrino interactions in the rock are identified using timing information. The times of hits along a reconstructed muon track are used to reconstruct the velocity $\beta = v/c$. Figure 5 shows the $1/\beta$ distribution for muon tracks of length greater than 2 m, where β is defined to be positive if the event is traveling downward. The large peak about $1/\beta = +1$ is due to downward going cosmic ray muons and has a width of $\sigma_{1/\beta} = 0.05$. The signal, neutrino induced upward-going muons, which is observed at $1/\beta = -1$ is clearly separated from the cosmic-ray background. A total of 58 events is selected.

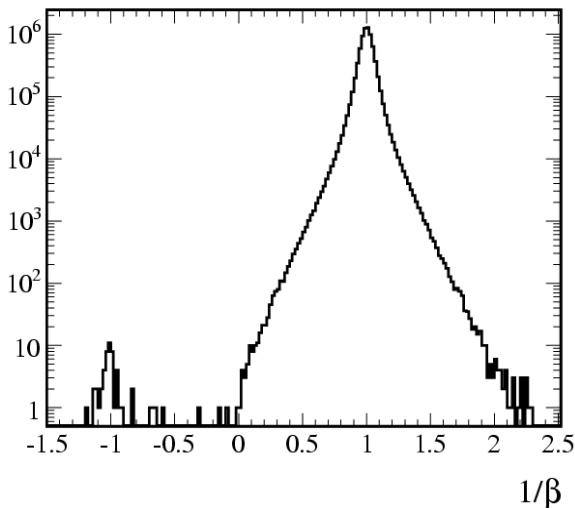


Figure 5. The distribution of $1/\beta$ ($\beta = v/c$) for reconstructed muon tracks of length greater than 2 m.

6.2. Contained events

At a depth of 2070 metres-water-equivalent (mwe) the cosmic ray muon background is approximately 50000 events per day in the MINOS detector. This rate should be compared to the expected signal rate of 0.30 ± 0.05 charged current $\nu_\mu/\bar{\nu}_\mu$ interactions per day. In order to achieve a signal-to-background ratio of greater than 10 it is necessary to identify efficiently the signal events while reducing the background by a factor of 10^6 .

Currently the analysis is restricted to fully-

contained events, *i.e.* in which the entire event is contained within the detector fiducial volume. The selection of fully-contained neutrino interactions was optimised using a GEANT 3 [14] simulation of the MINOS detector. For the simulation of atmospheric neutrino events the 3D flux calculation of Battistoni *et al.* [15] was used. The central sample was generated at solar maximum. The NEUGEN program [16] was used to simulate the neutrino interactions (cross-sections and hadronic final states). The interactions of hadronic particles were modelled with the GCALOR package.

The selection of fully contained CC $\nu_\mu/\bar{\nu}_\mu$ interactions proceeds in four main stages:

i) candidate contained events are required to have a reconstructed track spanning at least eight planes.

ii) events are defined as fully-contained if there is no significant activity outside the fiducial region. The fiducial volume is defined as the octagonal region which is at least 50 cm from the detector edges in the xy plane and at least 5 planes from the start of SM1 and end of SM2. The containment cuts reject approximately 99.9% of the cosmic ray background.

iii) After the above requirements, the dominant source of background comes from steep cosmic-ray muons which enter the detector at small angles to the xy -planes. Such events can penetrate a significant distance into the fiducial volume before leaving a detectable signal by travelling in the steel or air between the scintillator planes. A number of topological cuts are applied to reduce this category of background.

iv) After the above cuts a signal-to-background ratio of approximately unity is achieved. Requirements on hits in the veto shield are used to reduce the background to an acceptable level. The efficiency of the veto shield is estimated to be $96.6 \pm 0.4\%$. The estimated fraction of signal events rejected due to spurious veto shield hits is $2.2 \pm 0.4\%$, where the error represents systematic time dependent variations.

The event selection reduces the background from cosmic-ray muons by a factor of over 10^6 . The efficiency for genuinely contained events with a muon which traverses eight or more scintillator

planes is approximately 80%. The lower limit on the neutrino energy for selected events is approximately 0.5 GeV. From the 1.85 kt years exposure considered here 37 candidate contained events are selected (an example is shown in Figure 6).

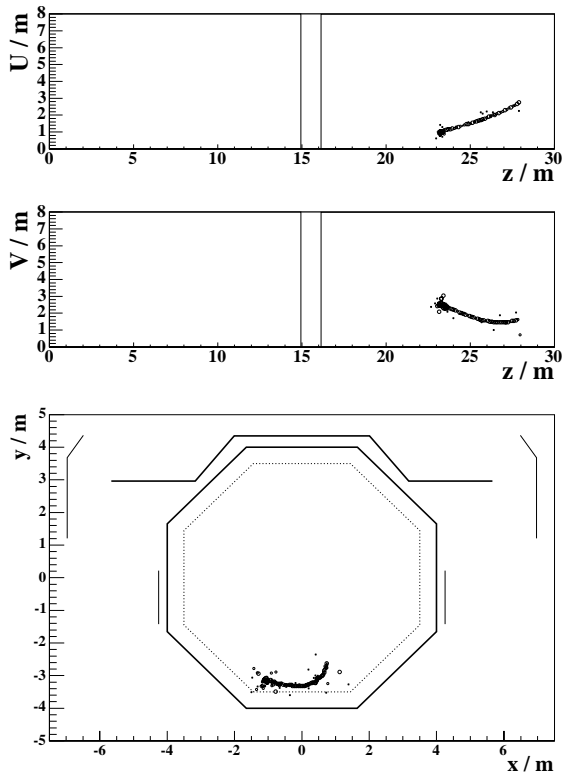


Figure 6. A selected fully-contained atmospheric neutrino event.

The numbers of events before and after the veto shield cuts are listed in Table 1. The final veto shield requirement rejects 51 events in data, consistent within one standard deviation with the Monte Carlo expectation of 61 ± 6 .

The 37 selected events are consistent with both the expectation of 40 ± 8 events assuming no neutrino oscillations, and with the expectation of 29 ± 6 events assuming $\Delta m_{23}^2 = 0.0025 \text{ eV}^2$ and $\sin^2 2\theta_{23} = 1.0$. The zenith angle distribution of the selected events is compared to the Monte Carlo expectation in Figure 7.

Table 1

Comparison of data and Monte Carlo before and after the veto shield requirements.

	Data	MC (no osc.)	MC Cosmic Background
Before Veto	88	39	63 ± 6
Vetoed	51	1	61 ± 6
Selected	37	38 ± 8	2

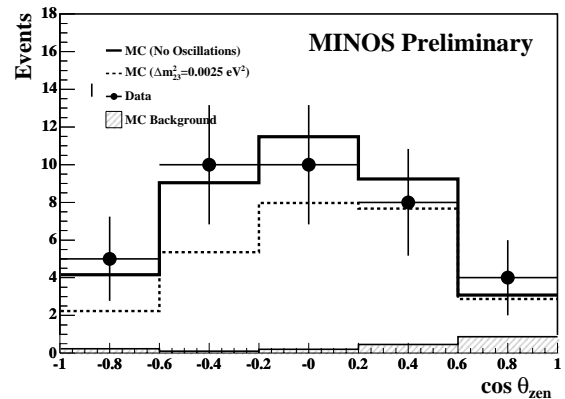


Figure 7. The reconstructed $\cos \theta_{\text{zen}}$ distribution for the 37 selected contained events compared to the MC expectation. The solid histogram shows the MC expectation for the case of no neutrino oscillations and the dashed histogram shows the expectation for $\nu_{\mu} \leftrightarrow \nu_{\tau}$ oscillations with $\sin^2 2\theta_{23} = 1.0$ and $\Delta m_{23}^2 = 0.0025 \text{ eV}^2$.

6.3. Separation into ν_{μ} and $\bar{\nu}_{\mu}$ interactions

From the point of view of atmospheric neutrino oscillations, the unique feature of the MINOS detector is the magnetic field. This opens up the possibility of identifying charged current neutrino events as either ν_{μ} or $\bar{\nu}_{\mu}$ interactions. However, an unambiguous identification is not possible for all events. The ability to identify the charge depends on the muon momentum, the track length in the detector and orientation with respect to the MINOS magnetic field. Table 2 gives a breakdown of the selected events into ν_{μ} and $\bar{\nu}_{\mu}$ interactions.

Table 2

Identification of the selected events as ν_μ , $\bar{\nu}_\mu$ or ambiguous.

	ν_μ	$\bar{\nu}_\mu$	$\nu_\mu/\bar{\nu}_\mu$?
Upward Muons	13	8	27
Contained Events	17	6	14

The reconstructed neutrino interaction vertex positions of the selected events (separated according to charge identification) are shown in Figure 8. Given the limited exposure no attempt is made to extract oscillation parameters from the data.

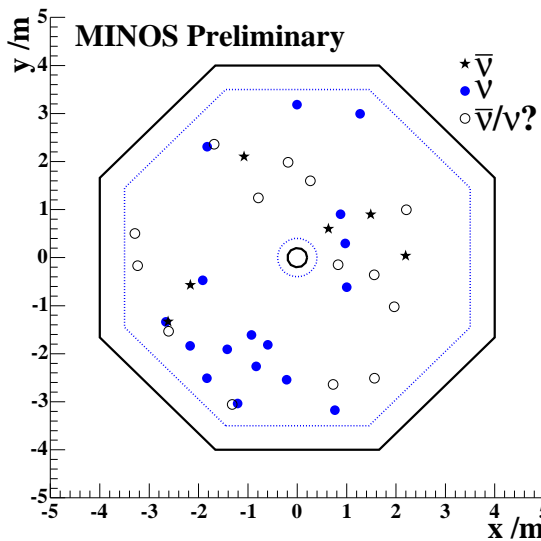


Figure 8. The xy positions of the interaction vertex for selected contained events.

7. Conclusions

Preparations for the MINOS long-baseline neutrino oscillation experiment are in an advanced state; first physics beam data is anticipated early 2005. The MINOS far detector has been recording high quality data for over a year. Using these data the first atmospheric neutrino interactions have been identified. These data will be used to make the first direct separate observations of ν_μ and $\bar{\nu}_\mu$ atmospheric neutrino oscillations. The next few years represent an exciting time for the MINOS collaboration and by the time of Neutrino 2006 we expect to have interesting results from both beam and atmospheric neutrino data.

REFERENCES

1. Super-Kamiokande Collaboration, Y. Fukada *et al.*, Phys. Lett. **B433** (1998) 9-18; Phys. Rev. Lett. **81** (1998) 1562–1567; Phys. Lett. **B436** (1998) 33–41; Phys. Lett. **B467** (1999) 185–193; Phys. Rev. Lett. **85** (1999) 2644–2648; Phys. Rev. Lett. **85** (2000) 3999–4003.
2. MACRO Collaboration, M. Ambrosio *et al.*, Phys. Lett. **B566** (2003) 35–44.
3. Soudan 2 Collaboration, M. Sanchez *et al.*, Phys. Rev. **D68** (2003) 113004.
4. Super-Kamiokande Collaboration, Y. Ashie, *et al.*, “Evidence for an oscillatory signature in atmospheric neutrino oscillation”, hep-ex/0404034, Submitted to Phys. Rev. Lett.
5. E. Kearns, “Atmospheric neutrino results from Super-Kamiokande”, elsewhere in these Proceedings.
6. MINOS Collaboration, P. Adamson, *et al.*, MINOS technical design report. NuMI-L-337, http://www.hep.anl.gov/ndk/hypertext/minos_tdr.html.
7. T. Nakaya, “K2K Results”, elsewhere in these Proceedings.
8. CHOOZ Collaboration, M. Apollonio *et al.*, Phys. Lett. **B466** (199) 415.
9. H. Murayama and T. Yanagida, Phys. Lett. **B520** (2001) 263.
10. G. Barenboim, L. Borissoff, J. L. Lykken and A. Y. Smirnov, JHEP **B0210** (2002) 001.
11. LSND Collaboration, A. Aguilar *et al.*, Phys. Rev. **D64** (2001) 112007.
12. M.C. Gonzalez-Garcia, M. Maltoni and T. Schwetz, Phys. Rev. **D68** (2003) 053007.
13. GCALOR, <http://www.physik.uni-mainz.de/zeitnitz/gcalor/gcalor.html>.
14. S. Giani *et al.*, “GEANT Detector Description and Simulation Tool”, CERN Program Library Long Writeup W5013.
15. G. Battistoni, A. Ferrari, T. Monturuli and P.R. Sala, Astropart. Phys. **19** (2003) 269; erratum *ibid* **19** (2003) 291.
16. NEUGEN program, version 3, H. Gallagher, Nucl. Phys. **B(Proc. Suppl.) 112** (2002) 188.